A FIELD EXPERIMENT ON GRAVITY WAVES: EFFECTS OF THE WAVE STEEPNESS AND EFFECTIVE WATER DEPTH ON THE WAVE PROFILE AND BREAKING LIMIT

George Spiliotopoulos[1], Vanessa Katsardi[1], Vincenzo Fiamma[2], Carlo Ruzzo[2], Alessandra Romolo[2], Felice Arena[2]

This paper describes a series of field observations of large surface gravity waves, recorded at the Natural Ocean Engineering Laboratory (NOEL), Italy. The study involves a variety of sea states measured at a series of water depths, from deep to the shallowest limit of intermediate waters. The discussion is focused on the effect of the spectral and local wave parameters, described by the wave steepness and the effective water depth, on the wave profile, statistical properties and the breaking characteristics. The data presented show a transition in the dispersive properties of the wavefield as waves propagate from deep to shallower water. This is indicated both in the wave profiles as well as the wave height distributions. Leading roles, albeit competitive to each other, play the wave steepness and wave breaking.

Keywords: Field Experiment; Random Waves; Probability of Exceedence; Finite water depths; Breaking Limit

INTRODUCTION

This paper describes field observations of limiting surface gravity waves, recorded at the Natural Ocean Engineering Laboratory (NOEL) of the Mediterranea University of Reggio Calabria, Italy. The experiment focuses on the evolution of a sea state as it propagates from deep to the shallowest limit of intermediate waters. The purpose of this experiment is to measure a large number of sea states evolving in a range of water depths. Due to the non-controlled nature of field experiments, the data was collected over a 2 month period between May and July 2023, a period ideal based on the local wind climate, in order to have a database consisting of the best possible variety of sea states. The goal of these measurements is to highlight the effects of the peak period, the wave steepness and the water depth on the wave profile and the breaking limit. Previous laboratory studies (e.g. Katsardi et al., 2013) have shown that the characteristics and formation of limiting waves are critically dependent on the effective water depth that reflects the peak period and the local water depth. These though were limited by the laboratory environment while the field conditions at NOEL can eliminate these weaknesses.

BACKGROUND

The NOEL has been a site for a multitude of field experiments, starting from Boccotti et al. (1993a,b); Boccotti (1997) and including Boccotti et al. (2011); Romolo and Arena (2013); Voermans et al. (2020). In these experiments, proof was derived for the quasi-determinism theory of Boccotti (1983), while the theory for the wave energy converter device, the so-called REWEC, was validated there as a scale model (Boccotti, 2007; Boccotti et al., 2007, 2012). The engineering significance of the findings from the experimental work in NOEL is presented in Boccotti (2014).

Regarding previous work relative to our research and concerning shallower water depths, Whittaker et al. (2016) analysed field data of surface water waves propagating on relatively shallow waters; the effective water depth ranging between $0.32 < k_p d < 0.48$. They have shown that the quasi-determinism or *NewWave* (Lindgren, 1970; Boccotti, 1983; Tromans et al., 1991) description of large waves may have some relevance even in this shallow water range. Nevertheless, the comparisons were made with the average linearised profile of the largest non-breaking measured waves. In the shallowest regions, the dispersive properties are limited, and the waves exhibit solitary-type behavior. Evidence for the latter is provided by field data presented in Tayfun and Alkhalidi (2020) involving severe sea states with large waves, including breaking waves, propagating at effective water depths between $0.19 < k_p d < 0.42$. Strong relevant evidence of the large waves' behaviour in the shallow end of intermediate waters is also shown in Katsardi et al. (2013).

It is well known that the effects on the formation of large waves are reflected in the statistical properties of the wavefield, such as the wave crest and height distributions (Gibson and Swan, 2007; Latheef and Swan, 2013) and the probability density functions (Fedele and Arena, 2010). While nonlinearity is very significant, wave breaking moderates its effects leading to a restriction of wave height, modifying the statistical properties of the wavefield (Latheef and Swan, 2013; Karmpadakis and Swan, 2020). Moreover, a number

[1]Department of Civil Engineering, University of Thessaly, Greece
[2]Natural Ocean Engineering Laboratory (NOEL), Mediterranea University of Reggio Calabria, Italy

of studies indicate that the relative importance of wave breaking increases as the effective water depth reduces. Examples include field data taken from four offshore locations (Wu et al., 2016) and laboratory data (Katsardi and Swan, 2011); all measured in finite water depth. Later, Karmpadakis et al. (2019) presented a series of wave basin laboratory measurements in intermediate water depths ($0.90 < k_p d < 1.80$), while Schubert et al. (2020) presented recently very long directional laboratory simulations of both breaking and non-breaking waves in a larger water depth range ($0.70 < k_p d < 2.26$). Statistical properties of waves recorded in NOEL are also presented in Voermans et al. (2020), concerning waves incident to a vertical wall.

Wave height distributions and breaking limits

The established wave height distributions that will be used in this paper are:

1. Rayleigh's linear distribution (Eq. 1) (Longuet-Higgins, 1953),

$$P_{cdf} = \exp\left[-2\left(\frac{H}{H_s}\right)^2\right] \tag{1}$$

2. Forristall (1978) linear distribution (Eq. 2) fitted to deep water data,

$$P_{cdf} = \exp\left[-2.263\left(\frac{H}{H_s}\right)^{2.126}\right] \tag{2}$$

3. Boccotti (1989) distribution (Eq. 3) that incorporates finite spectral bandwidth effects,

$$P_{cdf} = \frac{1 + \ddot{r}(T^*)}{\sqrt{2\ddot{r}(T^*)(1 - r(T^*))}} \exp\left[-\left(\frac{1}{4(1 - r(T^*))}\frac{H}{\sigma_\eta}\right)^2\right] \tag{3}$$

   with T^* being the abscissa of the first minimum of the autocorrelation function ($r(t)$) of the surface elevation and the double over dot denotes the second time derivative: $\ddot{r}(t) = \partial^2 r/\partial t$.

4. Klopman (1996) modified Glukhovskii distribution (Eq. 4) derived from field experiments:

$$P_{cdf} = \exp\left[-A\left(\frac{H}{H_{rms}}\right)^\kappa\right] \tag{4}$$

   H_{rms} is the root mean square wave height and κ is assumed to be a function of the ratio $H^* = H_{rms}/d$ such that:

$$\kappa = \frac{2}{1 - \beta H^*} \tag{5}$$

   and A is defined by:

$$A = \left[\Gamma\left(\frac{2}{\kappa} + 1\right)\right]^{\frac{k}{2}} \tag{6}$$

   Γ denotes the gamma function and $\beta = 0.7$ based on a fit from laboratory data (Klopman, 1996).

5. Battjes and Groenendijk (2000) composite weibull distribution (CWD) (Eq. 7):

$$P_{cdf} = \begin{cases} P_1(H) = \exp\left[-\left(\frac{H}{H_1}\right)^{k_1}\right] & H \le H_{tr} \\ P_2(H) = \exp\left[-\left(\frac{H}{H_2}\right)^{k_2}\right] & H \ge H_{tr} \end{cases} \tag{7}$$

   where $k_1 = 2$, $k_2 = 3.6$, and H_{tr} defines the transition wave height at which the Weibull distributions are matched. By defining the transition wave height as:

$$H_{tr} = (\beta_{tr1} + \beta_{tr2} m) d \tag{8}$$

   where $\beta_{tr1} = 0.35$ and $\beta_{tr2} = 5.8$. The solution includes the local water depth (d) and also the bottom slope (m). The normalising wave heights, H_1 and H_2, are expressed in terms of the normalised transition wave height, $\overline{H}_{tr} = H_{tr}/H_{rms}$ and given by an equation or tables from Battjes and Groenendijk (2000).

6. Mendez et al. (2004) distribution (Eq. 9) that also includes the parameter of the bed slope:

$$P_{cdf} = \exp\left[-\phi^2(\kappa^*)\left(\frac{\xi}{1-\kappa^*\xi}\right)^2\right] \text{ for } 0 \leq \xi \leq 1/\kappa^* \tag{9}$$

with $\xi = H/H_{rms}$, $\phi(\kappa^*) \simeq [1-(\kappa^*)^{0.944}]^{1.187}$ and κ^* as a single shape parameter dependent on the local wave properties and the propagation history and estimated with the following empirical equation:

$$\kappa^* = \left(\frac{H_{rms}}{d}\right)^{2.5}(4.7 - 20.8Ir + 26.2Ir^2) \tag{10}$$

where Ir is the local Iribarren number, $Ir = \sqrt{H_{rms}/(gT_m^2/2\pi)}$, m the bed slope and T_m the mean wave period.

The wave breaking limits that are used for comparisons in this paper are:

1. McCowan (1894) solitary wave breaking criterion ($H/d = 0.78$),
2. Miche (1944) criterion (Eq. 11), appropriate for regular waves and valid for all water depths,

$$\frac{H_b k}{2} = 0.142\pi \tanh(kd) \tag{11}$$

3. Goda (2010) updated criterion (Eq. 12) for incipient wave breaking,

$$\frac{H_b}{d} = 2\pi\frac{A}{k_o d}\left[1.0 - e^{-1.5\frac{k_o d}{2}(1+11m^{4/3})}\right] \tag{12}$$

k_o indicating the deep water wavenumber, m the bed slope and $A = 0.173$.

EXPERIMENTAL SETUP

At NOEL, the governing wind field (both fetch and velocities), as well as the local bathymetry characteristics, allows the conduction of field experiments with a length scale between 1:30-1:50 compared to open sea experiments, hence a time scale of 1:5-1:7. The local bed slope is ≈1:10. The measurements were carried out using a set of 7 ultrasonic probes over the mean water level and 5 pressure transducers underwater, all supported on 4 separate steel columns (Fig. 1). In this study, only the surface elevation data from the ultrasonic probes was used.

Key Parameters

The measured data allows the quantification and variation of the maximum crest elevation, the maximum wave height and the occurrence of wave breaking with respect to key parameters such as the significant wave height H_s, the spectral peak period T_p, and the local depth d. In physical terms the significant wave height and the spectral peak period determine the sea state steepness ($k_p H_s/2$), where k_p is the wave number corresponding to the spectral peak. The effective water depth ($k_p d$) is related to the water depth and the spectral peak period. Both parameters, the sea state steepness and the effective water depth, determine the nonlinearity of the wavefield and the extent of the occurrence of any wave breaking.

Processing field data

The time window chosen as representative of a storm in full scale conditions is 1h corresponding to approximately 5-7h for scale factors of 1:30-50, while the underlying spectra were extracted by using FFTs. The waves were analysed with a zero up-crossing method to extract individual wave properties. As shown in Fig. 1, there are two wave records measured at each water depth. The records chosen here are the least noisy compared to the ones in the same depth to ensure reliable results. In this case, the sensors chosen are the ones labeled U1, U3 and U6. The measured surface elevation data is stored in individual 5min records. By extracting the H_s of each such record (Fig. 2), we were able to assess time periods of significant wavefield steepness on several occasions throughout the length of the experiment, and then focus on those. Herein, we will examine three 1h records of significant wave activity and assess their properties. The records are named *rec140723*, *rec260723* and *rec270723*, corresponding to the dates they were collected and involve ≈1700 individual waves. The main analysis will be done on the steepest record *rec260723* with additional commentary on the other two.

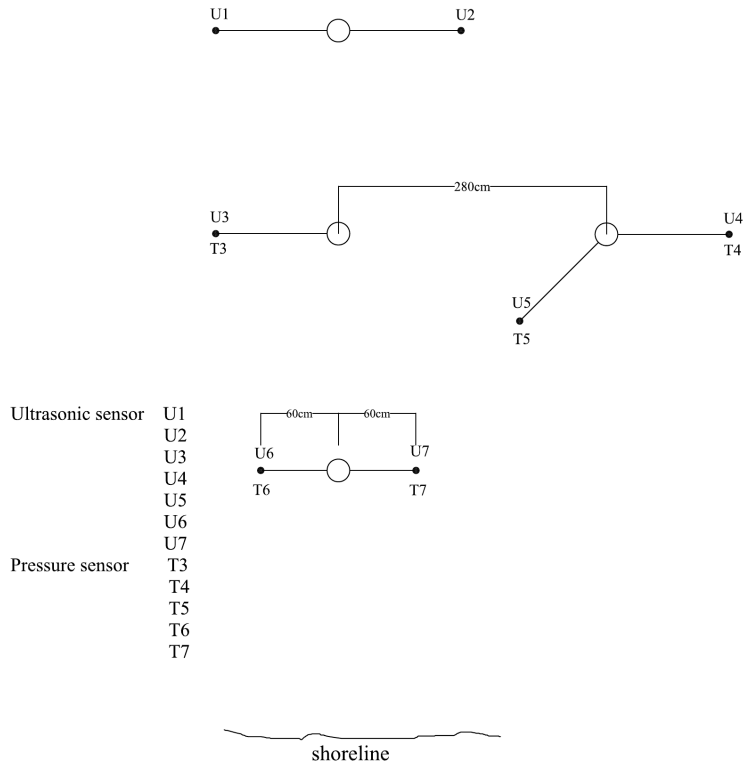

Figure 1: The arrangement of sensors

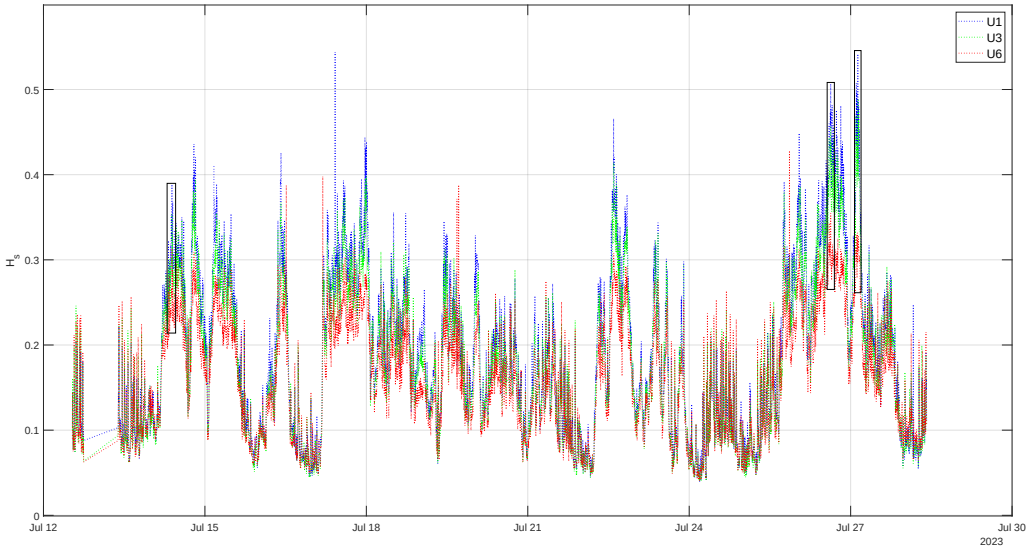

Figure 2: H_s per each individual 5min record in July 2023. The three records chosen are indicated with black rectangles

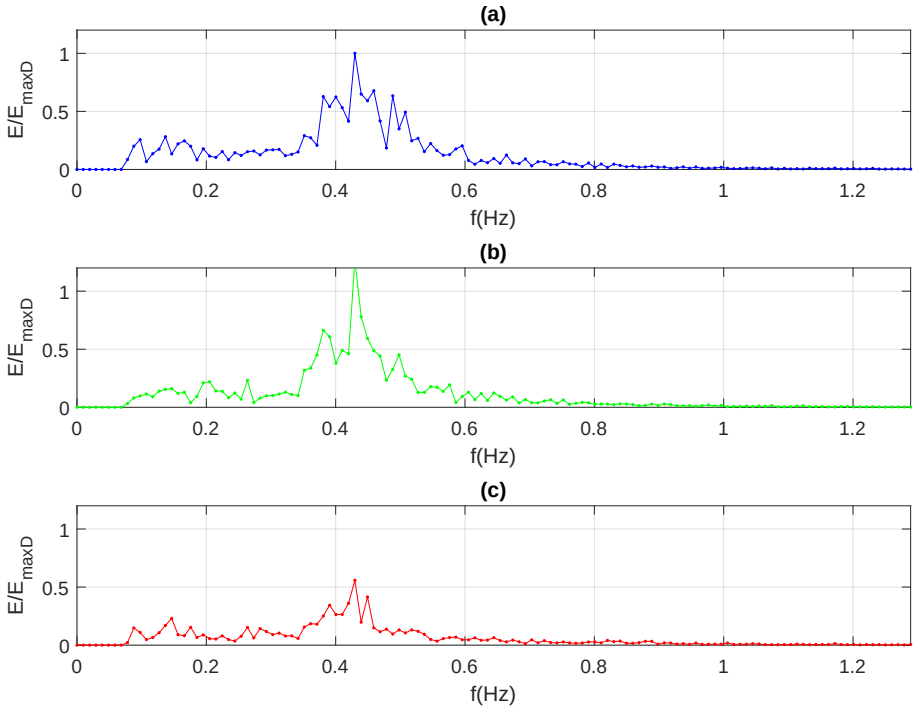

Figure 3: Energy density spectra of rec260723 (normalised with maximum of the deepest sensor), a) d = 3.86**m -** $k_p d$ = 2.89**, b)** d = 1.82**m -** $k_p d$ = 1.50**, c)** d = 0.54**m -** $k_p d$ = 0.68

DISCUSSION OF RESULTS

Table 1 provides the wavefield parameters for the three cases indicated in Fig. 2 which will be analysed in this Section.

Table 1: Wavefield parameters for the three cases

	rec140723			*rec260723*			*rec270723*		
Parameters	U1	U3	U6	U1	U3	U6	U1	U3	U6
Depth (in m)	3.78	1.75	0.44	3.86	1.82	0.54	3.83	1.79	0.50
T_p (in s)	2.63	2.84	2.84	2.33	2.33	2.33	2.84	2.84	3.01
$k_p d$	2.26	1.09	0.49	2.89	1.50	0.68	1.98	1.11	0.49
H_s (in m)	0.344	0.322	0.255	0.387	0.359	0.275	0.440	0.410	0.297
H_{rms} (in m)	0.223	0.214	0.176	0.251	0.234	0.184	0.288	0.270	0.200
$H_s k_p/2$	0.103	0.100	0.140	0.145	0.148	0.173	0.114	0.127	0.144
H_{max} (in m)	0.559	0.584	0.401	0.593	0.589	0.400	0.694	0.701	0.419

Frequency Spectrum

The extracted power density spectra for case *rec260723* are shown in Fig. 3. The spectrum is broad in deeper waters ($k_p d$ = 2.89) and becomes narrower in intermediate water depth ($k_p d$ = 1.50). In shallower water ($k_p d$ = 0.68) the wave energy has dissipated due to wave breaking. Note that k_p corresponds to the locally measured spectrum.

Wave Profile

In Fig. 4 the wave profile close to the largest measured wave height, H_{max}, of each record is displayed. The wavefield is relatively steep (deep water steepness $H_{so} k_p/2$ = 0.145) propagating from effectively deep to shallow waters ($2.89 \geq k_p d \geq 0.68$). By analyzing the wave profile in the different depths for this steep sea state, the different shapes in the largest waves are evident; in the larger water depth the wavefield is relatively dispersed, while the wavefield at the shallowest probe is much less dispersed and the largest

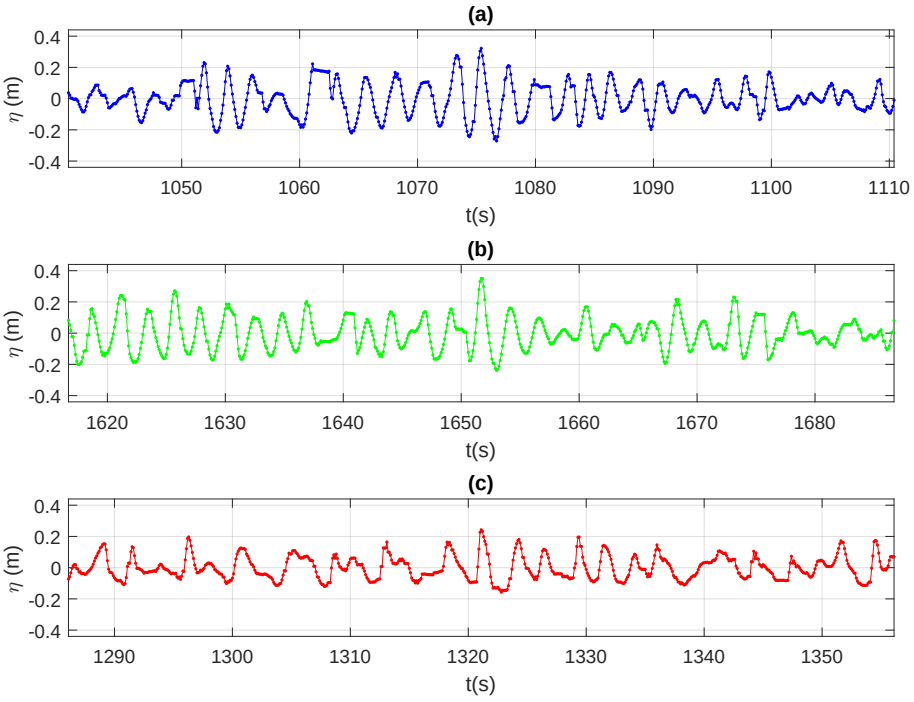

Figure 4: Wave profile close to H_{max} of *rec260723*, a) $d = 3.86$**m -** $k_p d = 2.89$**, b)** $d = 1.82$**m -** $k_p d = 1.50$**, c)** $d = 0.54$**m -** $k_p d = 0.68$

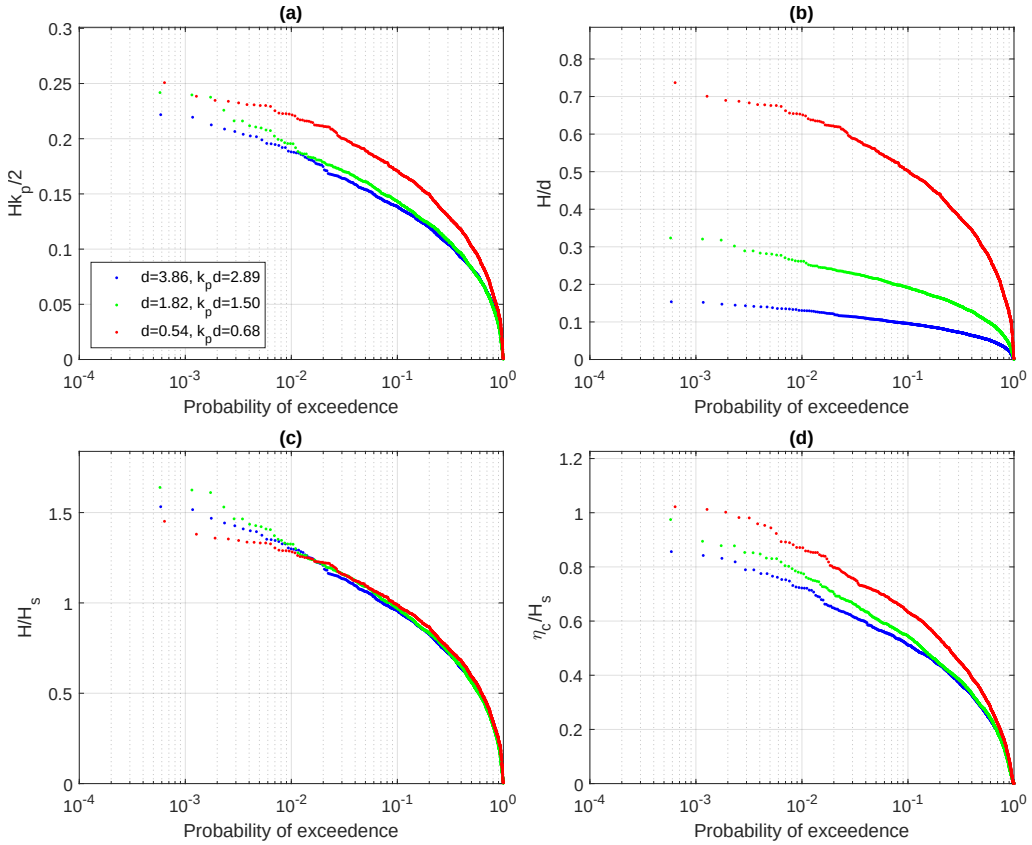

Figure 5: a) $Hk_p/2$**, b)** H/d**, c)** H/H_s **and d)** η_c/H_s **plotted against their probability of exceedence for *rec260723*:** $T_p = 2.33$**s,** $H_{so}k_p/2 = 0.145$

waves resemble a wave soliton. The above findings are consistent with previous extended experimental work by Katsardi et al. (2013).

Probability of exceedence

In Fig. 5 the wave steepness $Hk_p/2$, the H/d parameter, the H/H_s parameter and the η_c/H_s parameter are plotted against their probability of exceedence, Q, for the waves at each water depth level. Apparently in Fig. 5a there is an increase in wave steepness with the reduction of water depth, particularly in the shallowest record. Between the deep and intermediate records there is minimal increase in steepness that could be attributed to the shoaling process. Also, shallow water waves look to have reached some threshold due to wave breaking. This is also apparent in Fig. 5b , where in shallow water the H/d parameter reaches 0.75. In deeper waters H/d is small which reflects a wavefield that is not depth limited. In Fig. 5c, the deep and intermediate water distributions are similar with a slight increase of the H/H_s ratio for the intermediate depth reflecting the small increase in the wavefield steepness (Fig. 5a). However, the shallower distribution has a different shape, with the H/H_s ratio increasing for $Q > 2 * 10^{(-2)}$ and decreasing for $Q < 2 * 10^{(-2)}$ compared to the distributions in deep water. This is due to the competitive influence of the increase of both the wavefield steepness and wave breaking. Finally, Fig. 5d (η_c/H_s) shows the gradual increase in the crest-trough asymmetry as we move from deep to shallow water, directly related to the increase of nonlinearity or wave steepness.

Fig. 6 presents wave height distribution plots against their probability of exceedence (Q, H) compared with well-known distributions presented earlier in this paper. As seen in Fig. 6, in deep water, all of the distributions overestimate the wave heights, with Boccotti's and Klopman-Glukhowskii's showing the best behaviour. In intermediate water, all of the distributions overestimate the wave heights except for Klopman's. In shallower water, the Klopman-Glukhowskii still works well together with the Mendez distribution. In previous laboratory work by Katsardi et al. (2013), the best distribution in intermediate water depths

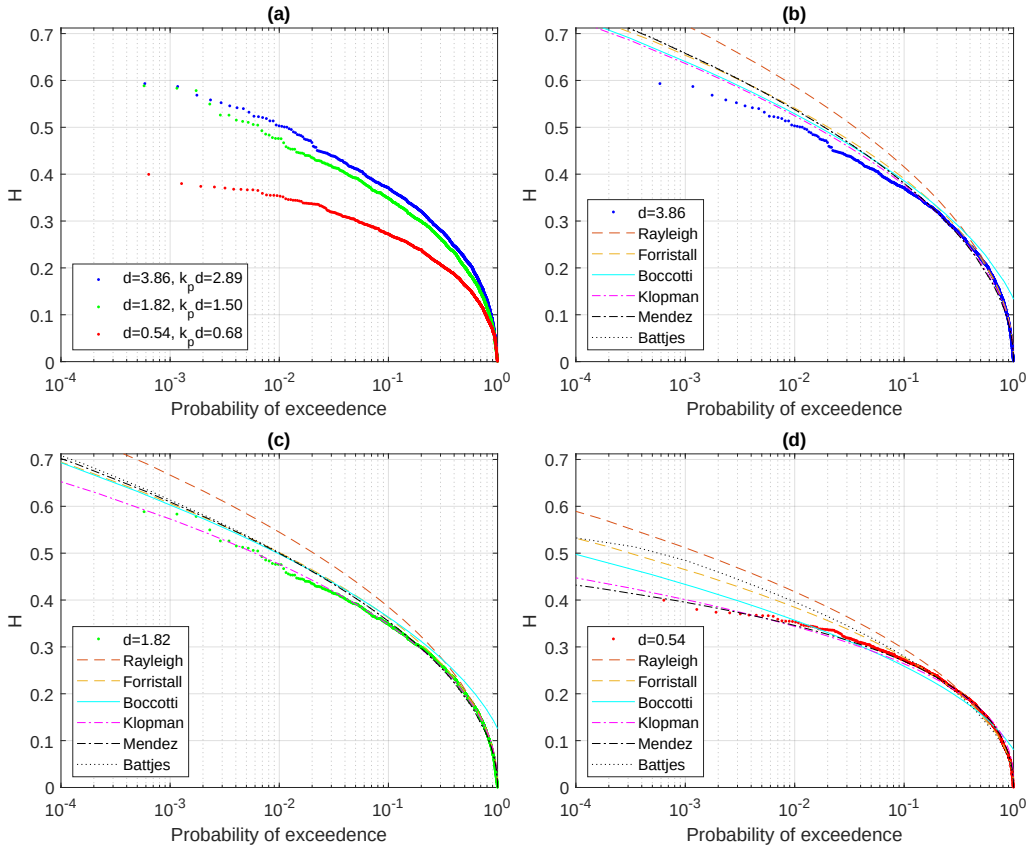

Figure 6: ***rec260723*****: a) Wave heights against probability of exceedence and wave height distributions for b)** $d = 3.86$**m -** $k_p d = 2.89$**, c)** $d = 1.82$**m -** $k_p d = 1.50$**, d)** $d = 0.54$**m -** $k_p d = 0.68$

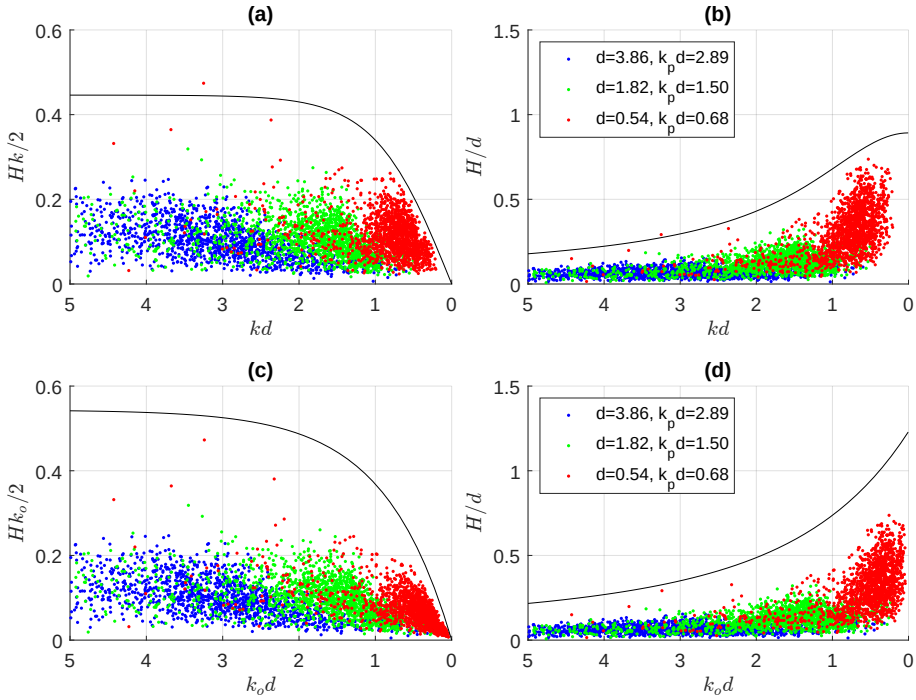

Figure 7: Variation of wave steepness ($Hk/2$) (a,c) and H/d per effective water depth (kd) for *rec260723* with Miche (a,b) and Goda (c,d) breaking criteria superimposed; (c,d) are based on deep water wavenumbers to align with Goda's criterion)

(similar to our $k_pd = 1.50$) was Battjes's distribution, while in shallower waters all distributions failed to describe wave heights with Klopman and Mendez showing better behaviour. However, the main differences of the laboratory experiment from this data set are that (i) it involves unidirectional wave propagation in a flume with all the additional dissipation limitations and (ii) it involves a much milder bed slope $m = 1/100$ compared to the field experiment ($m = 1/10$). Therefore, this shift in the validity of the distribution is probably due to the effect of the steeper bed slope and the related parameters such as the wave steepness (and thus the nonlinearity) and the effects of directionality. It is also significant to mention that the distributions that utilise the root-mean-square wave height (H_{rms}) are used with the measured H_{rms} from the dataset rather than estimations such as $H_{rms} = \frac{\sqrt{2}}{2}H_s$ according to linear theory for a narrow-banded process or other parametrisations that seem to overestimate the measured H_{rms}.

Wave Breaking

Fig. 7 describes the variation of the local wave steepness ($Hk/2$) and the wave height to water depth ratio (H/d) as a function of the local effective water depth from all $\sim$ 1700 separated waves from each sensor of *rec260723*. The Miche (1944) breaking criterion is superimposed with a black line on Fig. 7a,b and the Goda (2010) criterion on Fig. 7c,d. From the plot it is derived that in deep water the wavefield does not include breaking waves, but in shallow water the wavefield is much closer to breaking limit. In fact, some red dots that represent the shallow record are over the limit of the Miche criterion. On the other hand, Goda's limit, which includes the effect of bed slope, does not underestimate the largest waves occurring in shallow water. Propagating into shallower water the waves move even closer to the breaking limit, where each wave's local parameters are compared to the established breaking limits. Through spectral analysis (Fig. 3), there is also clear evidence of energy dissipation from wave breaking as spectral energy reduces significantly in the shallower measurements. Sometimes, a steeper sea-state in deep water can cause more energy dissipation prior to the waves reaching their more depth-limited state closer to the coast.

A shallower case with a rogue wave

In *rec140723*, whose local height maxima and surrounding wave profile are depicted in Fig. 8, the wavefield shows similar characteristics to *rec260723*, with the effective water depth of all records being

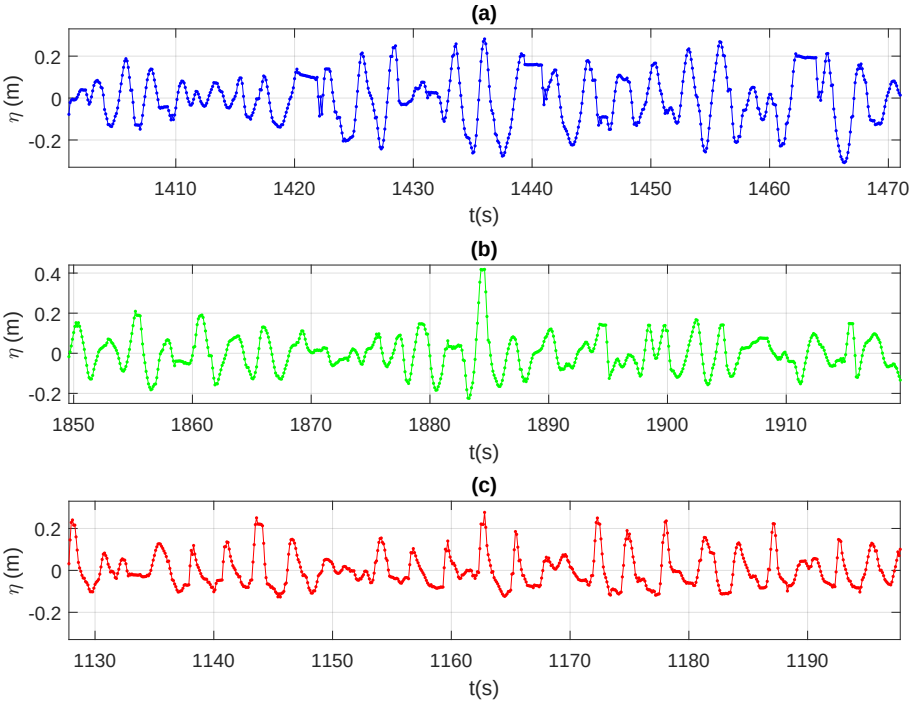

Figure 8: Wave profile close to H_{max} of *rec140723*, a) $d = 3.78$**m -** $k_p d = 2.26$**, b)** $d = 1.75$**m -** $k_p d = 1.09$**, c)** $d = 0.44$**m -** $k_p d = 0.49$

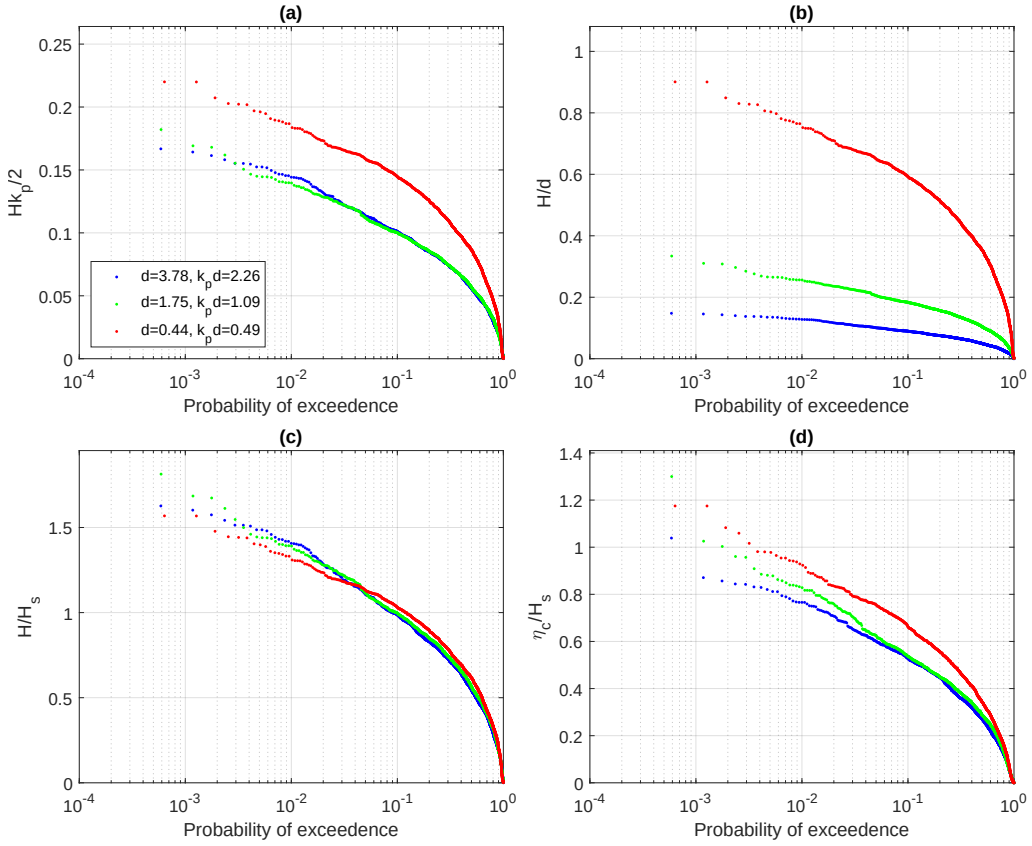

Figure 9: a) $Hk_p/2$**, b)** H/d**, c)** H/H_s **and d)** η_c/H_s **plotted against their probability of exceedence for *rec140723***

shifted shallower. Indeed, the shallowest record reaches the shallow limit $k_p d = 0.49 < 0.50$. This is profound in Fig. 8c where the wave profile, shows limited evidence of frequency dispersion but rather almost describes a sequence of solitary-type wave forms. This is consistent with the uni-directional laboratory measurements from Katsardi et al. (2013) discussed earlier in this paper. In the intermediate depth ($k_p d = 1.09$) record depicted in Fig. 8b there is the appearance of a rogue wave as defined by the $H \geq 2H_s$ criterion, as the downcrossing $H_{max} = 0.643\text{m} \simeq 2H_s$, the H_s being equal to 0.322m. It also satisfies the $\eta_c/H_s > 1.25$ threshold (Dysthe et al., 2008) as its crest height to significant wave height ratio reaches $\eta_c/H_s \simeq 1.3$.

As shown in Fig. 9a this wavefield is less steep than the previous one (Fig. 5a). It is interesting that the steepness in shallower water is significantly higher than the deeper records, where the steepness curves are almost identical. It is an indication of a wavefield that does not include a lot of breaking waves in deeper water, so the energy has not dissipated as much as a steeper wavefield when propagating into shallower water. The wave height to water depth ratio in shallow water (Fig. 9b) reaches $H/d > 0.78$, which is larger than the classic solitary wave McCowan (1894) breaking criterion. The contrast between these wave forms and those observed in deeper water (Fig. 8a) is marked, not least in terms of their crest-trough asymmetry. Indeed, it is hardly surprising that the distribution of wave heights and their limiting characteristics should differ significantly. In Fig. 9c the cross of the H/H_s curves indicate the limiting state of the dispersive characteristics of the wavefield, while the increase of the η_c/H_s ratio as the field propagates to shallower water is shown in Fig. 9d.

A case with large troughs on the highest waves

In *rec270723*, whose wave profile close to H_{max} is shown in Fig. 10, the effective water depth for all probes is similar with the *rec140723* case examined in Figs. 8, 9. Again, in shallower water (Fig. 11c) the wavefield has almost lost its dispersive characteristics, though in deeper water the local height maxima appear in instances with large troughs that resemble large regular waves that deviate from the usual shape of deep water large waves (Boccotti, 1983). As shown in Fig. 11a the shallower wavefield is as steep as *rec140723* but the deeper records show a wavefield that is much steeper in deeper water which has dissipated due to breaking when it reaches shallow water. In Fig 11b, the H/d ratio in shallower water also reaches $H/d > 0.78$, larger than the McCowan criterion. The H/H_s curves shown in Fig. 11c show a cross

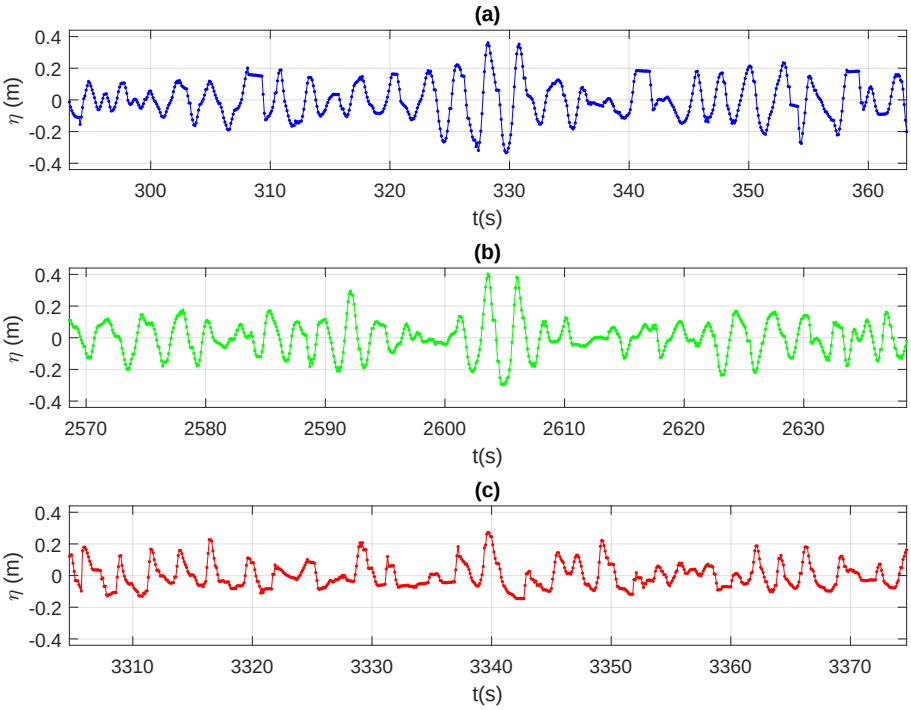

Figure 10: Wave profile close to H_{max} of *rec270723*, a) $d = 3.83$**m -** $k_p d = 1.98$**, b)** $d = 1.79$**m -** $k_p d = 1.11$**, c)** $d = 0.50$**m -** $k_p d = 0.49$

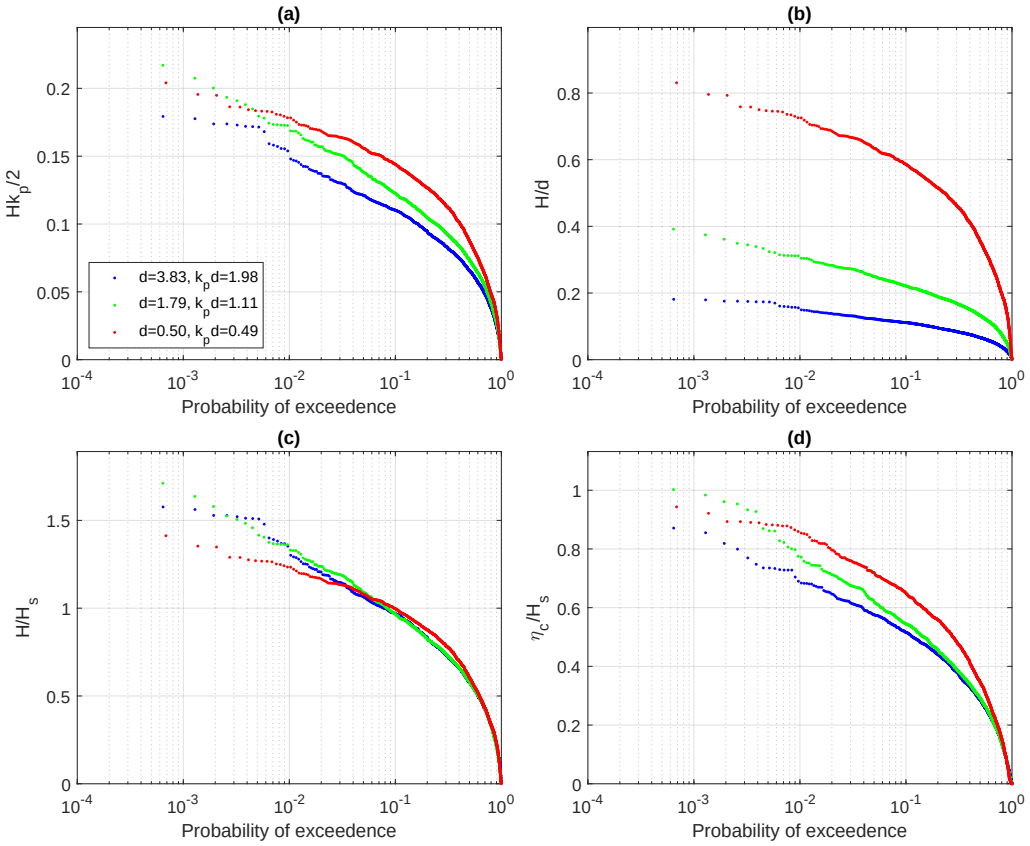

Figure 11: a) $Hk_p/2$**, b)** H/d**, c)** H/H_s **and d)** η_c/H_s **plotted against their probability of exceedence for** ***rec270723***

at steep angle of probability of exceedence between the shallower and deeper records that indicates again the difference in the dispersive properties as well as that the waves have reached a hard height threshold due to breaking. The threshold is also evident in Fig. 11d which shows the η_c/H_s curves.

CONCLUDING REMARKS

This work aims to provide evidence of the effects of the sea state and local wave parameters to the wave profile and wave breaking by using a dataset collected in the field that corresponds to real conditions. Previous numerical simulations and experimental findings are confirmed and enriched, showing the clear change in wave profile while steep waves are propagating in shallower water while they approach their breaking limit, with a soliton-like behaviour being the characteristic of shallower water steep waves. The main reason for this transition is the change in the dispersive properties of the wavefield, which is also indicated at the wave height distributions. Both wave steepness and wave breaking dominate the formation of the wave profile and the evolution of the wavefield albeit in a competitive manner. Finally, the bed slope seems to play a crucial role not only at the propagation and thus the increase in the wave height, but also in the calibration and validation of the various models; both related to probability of exceedence and breaking limit. More recent and elaborate wave and crest height distribution models (e.g. Wu et al., 2016; Karmpadakis et al., 2022; Karmpadakis and Swan, 2022) will be evaluated with this dataset in the future.

References

Noel – Natural Ocean Engineering Laboratory. https://noel.unirc.it/.

J. A. Battjes and H. W. Groenendijk. Wave height distributions on shallow foreshores. *Coastal Engineering*, 40(3):161–182, June 2000. ISSN 0378-3839. doi: 10.1016/S0378-3839(00)00007-7.

P. Boccotti. Some new results on statistical properties of wind waves. *Applied Ocean Research*, 5(3): 134–140, July 1983. ISSN 0141-1187. doi: 10.1016/0141-1187(83)90067-6.

P. Boccotti. On mechanics of irregular gravity waves. *Atti Accademia Nazionale dei Lincei, Memorie VIII,*, 19:111–170, 1989.

P. Boccotti. A general theory of three-dimensional wave groups Part I: The formal derivation. *Ocean Engineering*, 24(3):265–280, Mar. 1997. ISSN 00298018. doi: 10.1016/S0029-8018(96)00013-3.

P. Boccotti. Caisson breakwaters embodying an OWC with a small opening—Part I: Theory. *Ocean Engineering*, 34(5-6):806–819, Apr. 2007. ISSN 00298018. doi: 10.1016/j.oceaneng.2006.04.006.

P. Boccotti. *Wave Mechanics and Wave Loads on Marine Structures*. Marine Engineering. Butterworth-Heinemann, an imprint of Elsevier, Amsterdam Boston Heidelberg, 2014. ISBN 978-0-12-810258-9 978-0-12-800343-5.

P. Boccotti, G. Barbaro, V. Fiamma, L. Mannino, and A. Rotta. An experiment at sea on the reflection of the wind waves. *Ocean Engineering*, 20(5):493–507, Sept. 1993a. ISSN 00298018. doi: 10.1016/0029-8018(93)90017-C.

P. Boccotti, G. Barbaro, and L. Mannino. A field experiment on the mechanics of irregular gravity waves. *Journal of Fluid Mechanics*, 252:173–186, July 1993b. ISSN 0022-1120, 1469-7645. doi: 10.1017/S0022112093003714.

P. Boccotti, P. Filianoti, V. Fiamma, and F. Arena. Caisson breakwaters embodying an OWC with a small opening—Part II: A small-scale field experiment. *Ocean Engineering*, 34(5-6):820–841, Apr. 2007. ISSN 00298018. doi: 10.1016/j.oceaneng.2006.04.016.

P. Boccotti, F. Arena, V. Fiamma, A. Romolo, and G. Barbaro. Estimation of mean spectral directions in random seas. *Ocean Engineering*, 38(2-3):509–518, Feb. 2011. ISSN 00298018. doi: 10.1016/j.oceaneng.2010.11.018.

P. Boccotti, F. Arena, V. Fiamma, A. Romolo, and G. Barbaro. Small-Scale Field Experiment on Wave Forces on Upright Breakwaters. *Journal of Waterway, Port, Coastal, and Ocean Engineering*, 138(2): 97–114, Mar. 2012. ISSN 0733-950X, 1943-5460. doi: 10.1061/(ASCE)WW.1943-5460.0000111.

K. Dysthe, H. E. Krogstad, and P. Müller. Oceanic rogue waves. *Annual Review of Fluid Mechanics*, 40: 287–310, 2008. ISSN 1545-4479. doi: https://doi.org/10.1146/annurev.fluid.40.111406.102203.

F. Fedele and F. Arena. Long-Term Statistics and Extreme Waves of Sea Storms. *Journal of Physical Oceanography*, 40(5):1106–1117, May 2010. ISSN 1520-0485, 0022-3670. doi: 10.1175/2009JPO4335.1.

G. Z. Forristall. On the statistical distribution of wave heights in a storm. *Journal of Geophysical Research: Oceans*, 83(C5):2353–2358, 1978. ISSN 2156-2202. doi: 10.1029/JC083iC05p02353.

R. Gibson and C. Swan. The evolution of large ocean waves: The role of local and rapid spectral changes. *Proceedings of the Royal Society A: Mathematical, Physical and Engineering Sciences*, 463(2077):21–48, Jan. 2007. ISSN 1364-5021, 1471-2946. doi: 10.1098/rspa.2006.1729.

Y. Goda. Reanalysis of regular and random breaking wave statistics. *Coastal Engineering Journal*, 52(01): 71–106, Mar. 2010. ISSN 0578-5634. doi: 10.1142/S0578563410002129.

I. Karmpadakis and C. Swan. On the Average Shape of the Largest Waves in Finite Water Depths. *Journal of Physical Oceanography*, 50(4):1023–1043, Apr. 2020. ISSN 0022-3670, 1520-0485. doi: 10.1175/JPO-D-19-0165.1.

I. Karmpadakis and C. Swan. A new crest height distribution for nonlinear and breaking waves in varying water depths. *Ocean Engineering*, 266:112972, Dec. 2022. ISSN 00298018. doi: 10.1016/j.oceaneng.2022.112972.

I. Karmpadakis, C. Swan, and M. Christou. Laboratory investigation of crest height statistics in intermediate water depths. *Proceedings of the Royal Society A: Mathematical, Physical and Engineering Sciences*, 475(2229):20190183, Sept. 2019. ISSN 1364-5021, 1471-2946. doi: 10.1098/rspa.2019.0183.

I. Karmpadakis, C. Swan, and M. Christou. A new wave height distribution for intermediate and shallow water depths. *Coastal Engineering*, 175:104130, Aug. 2022. ISSN 03783839. doi: 10.1016/j.coastaleng.2022.104130.

V. Katsardi and C. Swan. An Experimental Study of Shallow Water Wave Statistics on Mild Bed Slopes. In *Volume 2: Structures, Safety and Reliability*, pages 711–719, Rotterdam, The Netherlands, Jan. 2011. ASMEDC. ISBN 978-0-7918-4434-2. doi: 10.1115/OMAE2011-49957.

V. Katsardi, L. De Lutio, and C. Swan. An experimental study of large waves in intermediate and shallow water depths. Part I: Wave height and crest height statistics. *Coastal Engineering*, 73:43–57, Mar. 2013. ISSN 03783839. doi: 10.1016/j.coastaleng.2012.09.007.

G. Klopman. Extreme wave heights in shallow water, Report H2486. Technical report, WLrDelft hydraulics, The Netherlands., 1996.

M. Latheef and C. Swan. A laboratory study of wave crest statistics and the role of directional spreading. *Proceedings of the Royal Society A: Mathematical, Physical and Engineering Sciences*, 469(2152): 20120696, Apr. 2013. ISSN 1364-5021, 1471-2946. doi: 10.1098/rspa.2012.0696.

G. Lindgren. Some Properties of a Normal Process Near a Local Maximum. *The Annals of Mathematical Statistics*, 41(6):1870–1883, Dec. 1970. ISSN 0003-4851, 2168-8990. doi: 10.1214/aoms/1177696688.

M. Longuet-Higgins. On the statistical distribution of the heights of sea waves. *Journal of Marine Research*, 11(3), Jan. 1953.

J. McCowan. XXXIX. On the highest wave of permanent type. *The London, Edinburgh, and Dublin Philosophical Magazine and Journal of Science*, 38(233):351–358, Oct. 1894. ISSN 1941-5982, 1941-5990. doi: 10.1080/14786449408620643.

F. J. Mendez, I. J. Losada, and R. Medina. Transformation model of wave height distribution on planar beaches. *Coastal Engineering*, 50(3):97–115, Jan. 2004. ISSN 0378-3839. doi: 10.1016/j.coastaleng.2003.09.005.

M. Miche. Mouvements ondulatoires de la mer en profondeur constante ou décroissante. *Annales de Ponts et Chaussées*, 114(1):131–164, 270–292, 369–406, 1944.

A. Romolo and F. Arena. Three-dimensional non-linear standing wave groups: Formal derivation and experimental verification. *International Journal of Non-Linear Mechanics*, 57:220–239, Dec. 2013. ISSN 0020-7462. doi: 10.1016/j.ijnonlinmec.2013.08.005.

M. Schubert, Y. Wu, J. Tychsen, M. Dixen, M. H. Faber, J. D. Sørensen, and P. Jonathan. On the distribution of maximum crest and wave height at intermediate water depths. *Ocean Engineering*, 217:107485, Dec. 2020. ISSN 0029-8018. doi: 10.1016/j.oceaneng.2020.107485.

M. A. Tayfun and M. A. Alkhalidi. Distribution of sea-surface elevations in intermediate and shallow water depths. *Coastal Engineering*, 157:103651, Apr. 2020. ISSN 0378-3839. doi: 10.1016/j.coastaleng.2020.103651.

P. S. Tromans, A. R. Anaturk, and P. Hagemeijer. A New Model For The Kinematics Of Large Ocean Waves-Application As a Design Wave. In *The First International Offshore and Polar Engineering Conf., Edinburgh*, International Ocean and Polar Engineering Conference, Aug. 1991.

J. J. Voermans, V. Laface, A. V. Babanin, A. Romolo, and F. Arena. Standing wave field observations at a vertical wall. *Coastal Engineering*, 160:103749, Sept. 2020. ISSN 0378-3839. doi: 10.1016/j.coastaleng.2020.103749.

C. N. Whittaker, A. C. Raby, C. J. Fitzgerald, and P. H. Taylor. The average shape of large waves in the coastal zone. *Coastal Engineering*, 114:253–264, Aug. 2016. ISSN 0378-3839. doi: 10.1016/j.coastaleng.2016.04.009.

Y. Wu, D. Randell, M. Christou, K. Ewans, and P. Jonathan. On the distribution of wave height in shallow water. *Coastal Engineering*, 111:39–49, May 2016. ISSN 03783839. doi: 10.1016/j.coastaleng.2016.01.015.